Publ. Astron. Obs. Belgrade No. 104 (2024), 169 - 174 *Progress Report*
https://doi.org/10.69646/aob104p169

MUSE-NFM OBSERVATIONS OF THE CIRCINUS ACTIVE GALACTIC NUCLEUS

SLADJANA KNEŽEVIĆ[1], DARSHAN KAKKAD[2], MARKO STALEVSKI[1,3], MAKOTO KISHIMOTO[4], DANIEL ASMUS[5,6] and FRÉDÉRIC P.A. VOGT[7]

[1] *Astronomical Observatory, Volgina 7, 11060 Belgrade, Serbia*
E–mail: sknezevic@aob.rs

[2] *Space Telescope Science Institute, 3700 San Martin Drive, Baltimore, MD 21218, USA*

[3] *Sterrenkundig Observatorium, Universiteit Gent, Krijgslaan 281-S9, Gent, 9000, Belgium*

[4] *Department of Astrophysics & Atmospheric Sciences, Faculty of Science, Kyoto Sangyo University, Kamigamo-motoyama, Kita-ku, Kyoto 603-8555, Japan*

[5] *Department of Physics & Astronomy, University of Southampton, Southampton, SO17 1BJ, UK*

[6] *Gymnasium Schwarzenbek, 21493 Schwarzenbek, Germany*

[7] *Federal Office of Meteorology and Climatology - MeteoSwiss, Chemin de l'Aérologie 1, 1530 Payerne, Switzerland*

Abstract. We present integral-field spectroscopic observations of the Circinus galaxy performed with the MUSE narrow field mode on the VLT. The spatial resolution of $\sim 0.1''$ within the field-of-view of $7.5'' \times 7.5''$ enabled us to zoom into the ionized gas kinematics within the central ~ 100 pc of the AGN. The analysis revealed that the systemic component resembles the ionization cone structure seen in larger scales, while the outflowing component shows a "tuning-fork" morphology: a collimated structure originating near the AGN location and extending in the north-western direction before it splits into two arms at around 30 pc from the AGN. We speculate that the origin of the collimated outflow might be due to the radio jet and ISM interactions on parsec scales, while a presense of a dust clump at the tip of the collimated part of the outflow might explain its fragmentation. The estimated total instantaneous and time-average mass outflow rates suggests that the observed outflow is not expected to regulate star formation within the ~ 100 pc. BPT diagram revealed that the dominant source of ionization is the AGN. In addition, we will present also the morphology and kinematics of the coronal gas traced by the high-ionization forbidden lines.

1. INTRODUCTION

Advancements in instrumentation over the past decades have yielded instruments with enhanced spectral and spatial resolution, facilitating more in-depth studies, particularly of nearby objects. One of these objects is Circinus, the closest Seyfert 2 galaxy (Freeman et al 1977). The active galactic nucleus (AGN) in this galaxy is oriented nearly edge-on, making it one of the best candidates to examine the outflows and test the standard toroidal obscuration model in the so-called unification scheme. High-resolution observations made in the mid-infrared wavelength range have revealed that infrared radiation from the polar regions, spanning distances of several parsecs (Tristram et al. 2014) to hundreds of parsecs (Asmus et al. 2016), dominates the total infrared energy budget of the AGN. The dust emission surrounding the Circinus'

AGN is believed to be composed of two distinct components, a thin equatorial disk and an extended polar feature that may arise from winds emanating from the central engine – the so-called polar-wind dust model (Stalevski et al. 2017, 2019). Recent polarimetric observations (Stalevski et al. 2023) also revealed dusty cone, i.e. hyperboloid with an half-opening angle of 40°, illuminated by a tilted geometrically thin accretion disk. Optical observations show a one-sided and a wide-angled kiloparsec ionization cone in the north west (Wilson et al. 2000, Mingozzi et al. 2019). In the upcoming sections, we will present the optical observations that resolve the regions close to the AGN torus with the aim to study co-spatial existence of dust and gas in the AGN.

2. OBSERVATIONS AND DATA ANALYSIS

We present observations of the Circinus' AGN (Kakkad et al. 2023) with the Multi Unit Spectroscopic Explorer (MUSE) in the narrow-field mode (NFM) with th Adaptive Optics (AO) on the Very Large Telescope (VLT). With a sampling of $0.025''$ per spatial pixel and a spatial PSF resolution $\sim 0.1''$, corresponding to 2 pc at a distance of 4.2 Mpc, we were able to resolve the region surrounding the AGN torus. The field-of-view of $7.5''\times7.5''$ allowed us to trace spatial scales up to nearly 100 pc from the AGN location. The wavelength coverage of 4800–9300Å was large enough to detect and study many lines including low, but also high-ionization forbidden lines. The spectral resolution was 150 kms^{-1} at [O III]λ5007 line, and the total exposure time around 4000 s on-source integration.

Data were reduced using the standard MUSE pipeline (Weilbacher et al. 2020). We applied the penalized pixel fitting (PPXF) routine (Cappellari 2017) to subtract the stellar continuum for which we employed modeled simple stellar populations (SSPs) from González Delgado et al. (2005), templates commonly used in the field for stellar continuum modeling up to approximately 7000Å. The following lines were analyzed: [O III]λ5007 for tracing the ionized gas, Hα and Hβ for dust extinction, [N II] doublet (6548Å and 6584Å) including the previous lines for determining the dominant source of ionization, [S II] doublet (6717Å and 6731Å) for estimating the electron gas density, and coronal lines ([Fe VII]λ6087, [Fe X]λ6375, [Ar V]λ7006) for investigating alternative ionization processes beyond those attributed to the AGN. We model the local continuum and the emission lines using the scipy.curve-fit package in *python* (Virtanen P. et al. 2020). All the lines were fitted with 1 or 2 Gaussians (see Figure 1), where the widths of the doublet lines were tied and their flux ratios fixed to the theoretical value. Also, the widths of Hβ and [N II] were tied to the width of [O III] and Hα line, respectively. We followed the non-parametric approach where we defined systemic component being inside $\pm300\,\mathrm{kms}^{-1}$ with respect to the line peak, and the outflow component outside this boundary. Also, we use v_{10} and w_{80}, blue-shifted velocity containing 10% and width containing 80% of the overall line flux, respectively.

3. RESULTS

3. 1. MORPHOLOGY AND KINEMATICS OF [O III]

The flux maps of the systemic and outflow components are shown in Figure 1. While the systemic component shows conical morphology, the outflow component is collimated and fragments into two arms forming a "tuning-fork" structure seen for the first time. We also show the residual map (right panel in Figure 1), i.e. the stellar velocity subtracted from the [O III] centroid velocity. The presence of residuals at the positions of the "tuning-fork" structure (red contours) implies that it is a constituent of the non-rotational component. The outflow co-rotates with the host galaxy and the ionized gas.

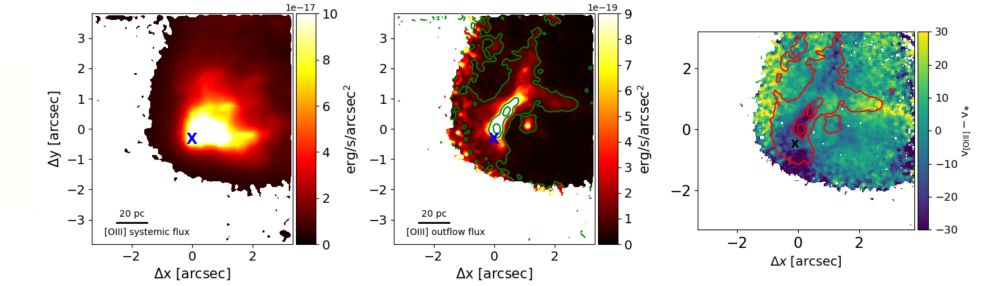

Figure 1: From left to right: systemic flux component, outflow flux component, subtracted stellar velocity map from the [O III] centroid velocity map. The blue sign "X" marks the AGN location. The middle-panel green and right-panel red contours are the [O III] outflow contours. The Figure is adapted from Kakkad et al. (2023).

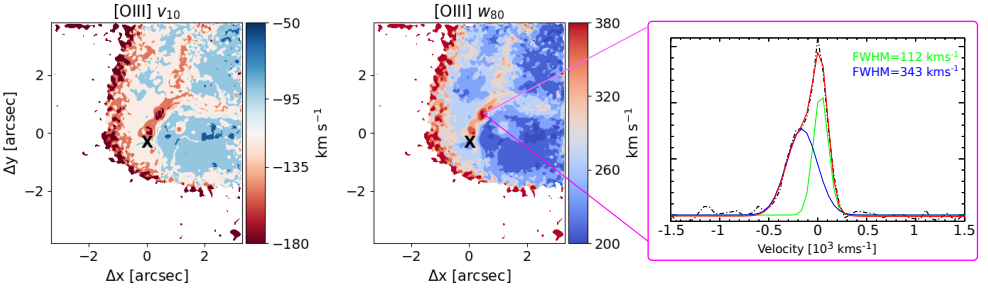

Figure 2: Left and middle panels show v_{10} and w_{80} distribution, respectively (taken from Kakkad et al. 2023). The blue sign "X" marks the AGN location. The right panel shows a spectrum in one of the spaxels belonging to the pointed outflow clump. Black dash-dotted line shows the stellar continuum corrected data, green and blue are the individual Gaussian components of the model for which the full width at half maximum (FWHM) are given in legend, and red line is the best-fit model.

In Figure 2 we present v_{10} and w_{80} maps showcasing blue-shifted (v_{10} mostly smaller than -150 kms^{-1}) and high-velocity (w_{80} mostly larger than 320 kms^{-1}) collimated outflow. The outflow is clumpy, having one clump already at around 8 pc from the AGN location, and at approximately 30 pc fragments into two arms. Clumps

show high blue-shifted (v_{10} < -180 kms^{-1}) and high velocity (w_{80} > 380 kms^{-1}) components.

We derive mass outflow rates from [O III]λ5007 line luminosity (Kakkad et al. 2023), where we use outflow flux ratio of [S II] doublet to estimate median outflow density of $\sim$200 cm^{-3}. We calculated both the instantaneous ($\dot{M}_{inst}$=10^{-2}M$_\odot$ yr^{-1}) and time-averaged mass outflow rate ($\dot{M}_{Tavg}$=10^{-4}M$_\odot$ yr^{-1}), where the former is the sum of the mass and velocity outflow product in every pixel, while in the latter we use the total outflow mass and the average velocity over the outflow region. Both values are much smaller than the star formation rate in Circinus reported in the literature, suggesting the observed ionized outflow is not expected to shut down star formation in parsec scale.

3. 2. BPT DIAGRAM AND DUST EXTINCTION

We construct Baldwin, Phillips & Terlevich (BPT) diagram using log flux ratios of [O III]/Hβ and [N II]/Hα. It is evident that the AGN is the dominant source of ionization and ionization by star formation (SF) is negligible. The shown maps are for the total line fluxes, but we get similar results for systemic and outflow fluxes. Thus, based on current observations, it appears that outflows are not playing a role in triggering SF near the AGN.

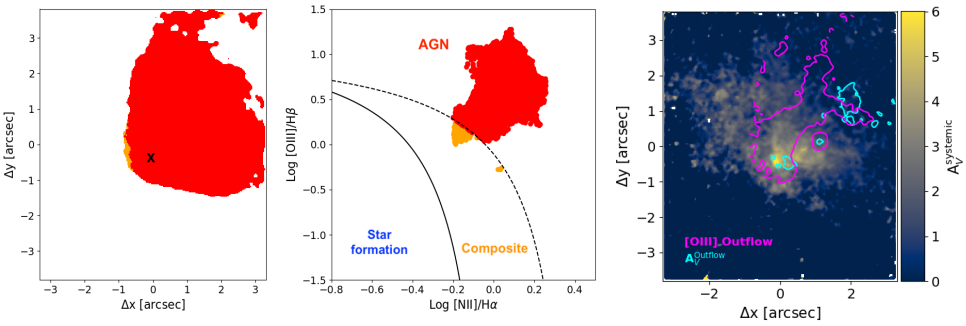

Figure 3: The first two panels show spatially resolved BPT diagram where red and blue are AGN and SF source of ionization, respectively. The third panel is the dust extinction map of the Circinus galaxy with yellow being the extinction obtained from the systemic component and cyan from the outflow component. The magenta contours are [O III] gas outflow. The Figure is adapted from Kakkad et al. (2023).

Next, we use Hα and Hβ luminosities, assuming Calzetti et al. (2000) dust attenuation law with R$_v$=4.05 and T$_e$=10 000 K, to derive dust extinction map in the Circinus galaxy (right panel in Figure 3). The extinction calculated from the systemic component reveals conical morphology with the equatorial disk. The extinction from the outflow component shows clumps with one clump being close to the site of outflow fragmentation into two arms and possibly causing the split. Radio images on larger scales (Elmouttie et al. 1998) reveal potential jet-like activity. Extrapolating its direction toward AGN location, we find it to be close to the ionization-cone edge, and we speculate the origin of the collimated outflow could be due to a pc-scale radio jet ISM interaction. However, high-resolution radio images are needed to make any firm conclusion.

3. 3. CORONAL LINES

Coronal lines such as [Fe VII], [Fe X], [Ar V] are also observed in our data set (see Figure 4) with the brightest emission close to the ionization-cone edge. These lines have already been detected in MUSE wide-field mode data (Fonseca-Faria et al. 2021).

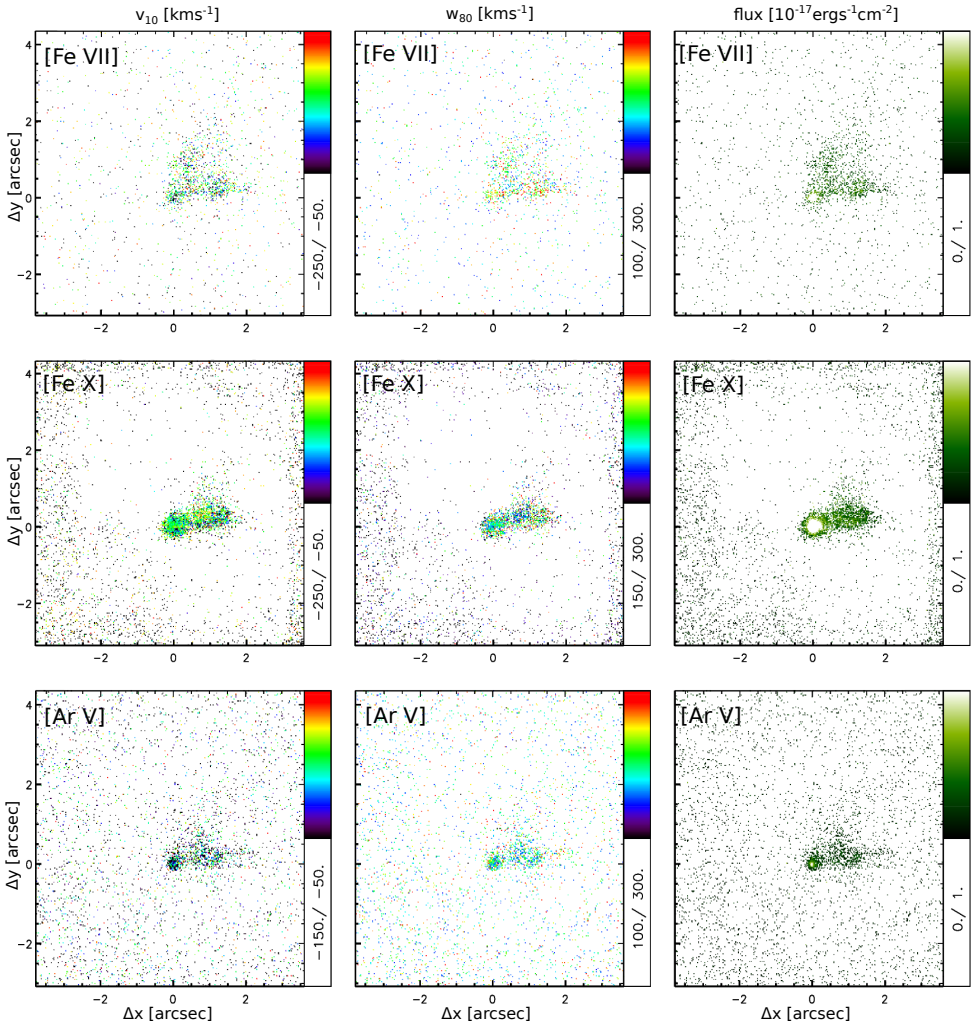

Figure 4: Coronal line parameters v_{10} (left), w_{80} (middle) and total flux (right) for [Fe VII] (top row), [Fe X] (middle row) and [Ar V] (bottom row).

The extended emission of these forbidden high-ionization lines up to 700 pc for [Fe VII] and [Ar V], and 400 pc for [Fe X] from the AGN cannot be explained only with the ionization from the central source. Ferguson et al. (1997) calculated the maximum distance of high ionization lines from the central ionization source. Their model predicts an upper limit of 110 pc distance from the AGN for [Fe VII] and 20 pc (or 1″ in our data set) for [Fe X] line. Therefore, there must be some additional mechanism to power coronal emission far from the AGN. The plausible explanation could be a

shock-driven coronal gas scenario. This scenario assumes that the jet in the Circinus galaxy induces shocks capable of ionizing gas at larger distances. The origin of the coronal lines within ~ 50 pc from the AGN and their relationship to the same lines observed at significantly greater distances will be investigated in the future.

4. SUMMARY AND FUTURE WORK

We presented VLT/MUSE NFM observations that resolved the regions close to the AGN torus (spatial resolution of 2 pc). We derived the properties of the ionized gas outflow using the [O III]λ5007 emission line, showing the conical morphology of the systemic [O III] component co-rotating with the host galaxy, and "tuning-fork" structure seen for the first time in the outflowing [O III] flux distribution, v_{10} and w_{80} maps. The high-velocity outflow is blue-shifted. Our estimates showed that the AGN is the dominant source of ionization, and that the ionized gas outflow is not expected to regulate star formation within a radius of ~ 100 pc from the AGN location. Systemic Balmer decrement shows the dust distribution concentrated along the ionization cone, while the outflowing decrement shows a clump at the fragmentation site. We speculate that the possible origin of the collimated outflow might be a small scale radio jet interaction with the ISM. Finally, we also presented parameter estimation for [Fe VII], [Fe X] and [Ar V] coronal lines. Further investigation is needed to connect them with the same lines observed on larger scales where shock excitation seems to play an important role.

Acknowledgments

Based on observations from the ESO programme ID 0103.B-0396. M.S. and S.K. acknowledge support by the Science Fund of the Republic of Serbia, PROMIS 6060916, BOWIE and by the Ministry of Science, Technological Development and Innovation of the Republic of Serbia through contract No. 451-03-66/2024-03/200002. D.A. acknowledges funding through the European Union's Horizon 2020 and Innovation programme under the Marie Sklodowska-Curie grant agreement no. 793499 (DUSTDEVILS).

References

Asmus, D., Hönig, S. F., Gandhi, P.: 2016, *ApJ*, **822**, 109.
Calzetti, D., Armus, L., Bohlin, R. C., et al.: 2000, *ApJ*, **533**, 682.
Cappellari, M.: 2017, *MNRAS*, **2466**, 798.
Elmouttie, M., Haynes, R. F., Jones, K. L., et al.: 1998, *MNRAS*, **297**, 1202.
Ferguson, J. W., Korista, K. T., Ferland, G. J.: 1997, *ApJS*,**110**, 287.
Fonseca-Faria, M. A., Rodríguez-Ardila, A., Contini, M., et al.: 2021, *MNRAS*, **506**, 3831.
Freeman, K. C., Karlsson, B., Lynga, G., et al.: 1977, *A&A*, **55**, 445.
González Delgado, R. M., Cerviño, M., Martins, L. P., et al.: 2005, *MNRAS*, **357**, 945.
Kakkad, D., Stalevski, M., Kishimoto, M., et al.: 2023, *MNRAS*, **519**, 5324.
Mingozzi, M., Cresci, G., Venturi, G., et al.: 2019, *A&A*,**622**, A146.
Stalevski, M., Gonzaléz-Gaitán, S., Savić, Dj., et al.: 2023, *MNRAS*, **519**, 3237.
Stalevski, M., Asmus, D., Tristram, K. R. W.: 2017, *MNRAS*, **472**, 3854.
Stalevski, M., Tristram, K. R. W., Asmus, D.: 2019, *MNRAS*, **484**, 3334.
Tristram, K. R. W., Burtscher, L., Jaffe, W., et al.: 2014, *A&A*, **563**, A82.
Virtanen, P., Gommers, R., Oliphant, T. E., et al.: 2020, *Nature Methods*, **17**, 261.
Weilbacher, P. M., Palsa, R., Streicher, O., et al.: 2020, *A&A*, **641**, A28.
Wilson, A. S., Shopbell, P. L., Simpson, C., et al.: 2000, *AJ*, **120**, 1325.